Resilience-Oriented Design of Distribution Systems

Shanshan Ma, *Student Member, IEEE,* Shiyang Li, *Member, IEEE,* Zhaoyu Wang, *Member, IEEE,*
Feng Qiu, *Senior Member, IEEE*

Abstract—Climatic hazards, such as hurricanes and ice-storms, pose a top threat to power distribution systems. This paper proposes a resilience-enhancing strategy to make distribution systems more resilient to climatic hazards. The proposed strategy consists of three resilience-oriented design (ROD) measures, namely line hardening, installing backup distributed generators (DGs), and adding automatic switches. The main challenges of this problem are i) modeling the spatio-temporal correlation among ROD decisions and uncertainties, ii) capturing the entire failure-recovery-cost process, and iii) solving the resultant large-scale mixed-integer stochastic problem efficiently. To deal with these challenges, we propose a hybrid stochastic process with deterministic casual structure to model the spatio-temporal correlations of uncertainties. A new two-stage stochastic mixed-integer linear program (MILP) is formulated to capture the impacts of ROD decisions and uncertainties on system's responses to climatic hazards. The objective is to minimize the ROD investment cost in the first stage and the expected costs of loss of load, DG operation, and damage repairs in the second stage. A dual decomposition (DD) algorithm with branch-and-bound is developed to solve the proposed model with binary variables in both stages. Case studies on the IEEE 123-bus test feeder show the proposed approach can improve the system resilience at minimum costs.

Index Terms—Distribution systems, dual decomposition, spatio-temporal correlated uncertainty, resilience-oriented design, stochastic mixed-integer programming

NOMENCLATURE

Sets and Indices

Ω_B	Set of line indices (i,j)
Ω_K	Set of hardening pole type indices k
Ω_L	Set of loads indices i
Ω_N	Set of nodes indices i
$\Omega_{\mathcal{S}}$	Probability space of stochastic scenarios
$\mathcal{S}$	Set of sampled scenario indices s
$\mathcal{T}_H$	Time duration set of climatic hazard indices t
ξ	A random event

Parameters

α_L	Penalty coefficient of virtual load
B'_{ij}	Virtual reactance for line (i,j)
c^c_{ij}	Cost of installing sectionalizer at line (i,j)
$c^h_{ij,k}$	Cost of hardening line (i,j) with k-th pole type
c^g_i	Cost of installing a DG at bus i
c^L_i	Cost of shedding $1kWh$ of i-th load
c^o_i	Cost of operating DG at bus i

m_{ij}	The total number of poles at line (i,j)
M_1, M_2	Sufficiently large positive numbers
M_3, M_4	Sufficiently large positive numbers
N_G	The limit for total number of newly installed DGs
$P^{L,s}_{i,t}, Q^{L,s}_{i,t}$	Stochastic parameter indicating active/reactive load demand at time t
$P^{\max}_{ij,t}, Q^{\max}_{ij,t}$	Maximum Active/reactive line flow at time t
$P^{g,\max}_i, Q^{g,\max}_i$	Active/reactive power limits of DG
R^e_{ij}, X^e_{ij}	Resistance/reactance of line (i,j)
S_0	Positive base power
V_0	Reference voltage magnitude
$V^{\max}_i, V^{\min}_i$	Maximum/minimum voltage magnitude
$\varepsilon_1, \varepsilon_2, \varepsilon_3$	Sufficiently small positive numbers
w_H	The total occurrence of climatic hazards in a year
$\chi^s_{ij,k}$	Stochastic parameter indicating repair cost of line (i,j) with k-th pole type
$x^{c_0}_{ij,i}$	Binary parameter indicating whether line (i,j) has an existing sectionalizer (1) or not (0) at the end i
$\zeta^s_{ij,k,t}$	Stochastic parameter indicating status of line (i,j) with k-th pole type, damaged (1) or functional (0) at time t

Variables

$c^{r,s}_{ij}$	Repair cost of line (i,j)
$\lambda^s_{a,ij,t}, \lambda^s_{b,ij,t}$	Dual variable
$\lambda^s_{c,i,t}$	Dual variable
$\mu^s_{d,i,t}, \mu^s_{e,i,t}$	Dual variable
$P^s_{ij,t}, Q^s_{ij,t}$	Active/reactive power flow of line (i,j) at time t
$P^{g,s}_{i,t}, Q^{g,s}_{i,t}$	Active/reactive power output of DGs at time t
$\mathcal{P}^s_{l,ij,t}$	Virtual line flow of line (i,j) at time t
$\mathcal{P}^s_{L,i,t}$	Virtual load of bus i at time t
$\theta^s_{i,t}$	Voltage angle (radians) at bus i at time t
$u^s_{ij,t}$	Binary variable indicating whether line (i,j) is damaged (1) or not (0) at time t
$V^s_{i,t}$	Voltage magnitude of bus i at time t
$w^{a,s}_{i,t}$	Binary variable indicating whether voltage angle is zero (1) or not (0) at bus i at time t
$w^{b,s}_{ij,t}$	Binary variable indicating whether line (i,j) is an active branch (1) or not (0) at time t
$w^{m,s}_{i,t}$	Auxiliary binary variable for setting different restriction on the voltage magnitude at bus i at time t
$w^{o,s}_{ij,t}$	Binary variable indicating whether line is on (1) or off (0) at time t
$x^{c_1}_{ij,i}$	Binary variable indicating whether a new sec-

tionalizer is deployed (1) or not (0) at the end i of line (i,j)

$x_{ij,i}^c$ Binary variable indicating whether line (i,j) has a sectionalizer (1) or not (0) at the end i of line (i,j)

$x_{ij,k}^h$ Binary variable indicating whether line (i,j) is hardened with k-th pole type (1) or not (0)

x_i^g Binary variable indicating whether a new DG is placed at bus i (1) or not (0)

$y_{ij,t}^{c,s}$ Binary variable indicating whether the sectionalizer at line (i,j) is open (1) or not (0) at time t

$y_{i,t}^{r,s}$ Load shedding percentage of load at bus i at time t

I. INTRODUCTION

RESILIENCE is the ability to prepare for, absorb, adapt to, and/or rapidly recover from adverse events [1]. Recent severe power outages caused by climatic hazards have highlighted the importance and urgency to improve the resilience of electric distribution systems. For example, between 2003 and 2012 roughly 679 power outages, each affecting at least 50,000 customers occurred due to weather events in the U.S., and $80\% - 90\%$ of these outages were due to distribution system failures [2]. The efforts to enhance distribution system resilience can be classified into two broad categories [3]–[5]: the planning and the operational methods. The operational methods include, for example, the proactive preparation [6]–[8] and the outage restoration [9], [10]. The ROD is a planning method that has drawn research interests in recent years [11]–[14]. In [11], a two-stage robust optimization-based decision support tool is proposed for designing a resilient distribution network, where a polyhedral set represents the line damage uncertainty. The cardinality budget for the number of damaged lines does not consider component fragility models, and only one ROD option, i.e., line hardening, has been considered. A tri-level robust optimization model considering grid component fragility models is proposed in [12]. However, due to the limitations of robust modeling, some ROD methods, such as upgrading distribution poles, and installing backup DGs and automatic switches, are not considered. References [13] and [14] formulate the ROD problem as two-stage stochastic mixed-integer programs. The work in [13] has improved previous works by considering the fact that the hardened lines would be damaged at a lower rate; however, the interdependence between the line hardening decisions and the line damage uncertainty is missed. Our previous work in [14] models this interdependence but the fragility model does not consider different pole types and temporal correlations of damages. Moreover, previous works assume a pole's physical damage only affects the line connected to the pole and neglects the potential outage propagation.

The primary challenge of distribution system ROD is to model the entire failure-recovery-cost process. Specifically, evaluating the damage states requires the modeling of various spatial-temporal uncertainties in weather events and structural strengths, and some of them are decision-dependent. The recovery phase is usually neglected in the existing literature on ROD. However, the ROD decisions affect the system recovery and the associated outage/repair costs. For example, adding DGs and switches offer self-healing capabilities such as reconfiguration and automatic microgrid formation. These self-healing actions are time-varying and should be modeled in the ROD problem. In addition, the outage induced by physical damages may propagate in the network until a sectionalizer isolates the fault. This interaction between structural damages and electric outage propagation should be modeled in the ROD problem.

To this end, the key contributions of the paper include:

- A hybrid independent stochastic process and deterministic causal structure is proposed to capture the spatiotemporal correlation among various uncertainties of a ROD problem. This approach avoids establishing the high-dimension joint distribution of uncertain variables.
- A simulation technique based on structural engineering is presented to model the evolving impacts of hurricanes on physical infrastructures to support a more accurate uncertainty modeling.
- A two-stage stochastic MILP is proposed to optimally implement multiple resilience-enhancing methods considering various uncertainties, thus increasing the infrastructure strength and enabling self-healing operations. Besides, this model captures the entire failure-recovery process so that both investment and restoration costs can be modeled.
- The self-healing operation in the second stage can mimic the outage propagation in the network until sectionalizers disconnect lines. The model sectionalizes a distribution system into multiple self-supported microgrids (MGs) and re-dispatches DGs to minimize the cost of the loss of load and DG operation in the second stage while keeping radial topologies.
- A customized dual-decomposition (DD) algorithm is developed to balance the optimality and the solution efficiency.

In summary, the main contribution of the paper is to develop a general planning model and solution algorithm for enhancing distribution system resilience. The rest of the paper is organized as follows. Section II provides the problem statement. Section III proposes a mathematical formulation of ROD problems and presents a new solution algorithm. Numerical results are shown in Section IV. Section V concludes the study of our work.

II. PROBLEM STATEMENT

In this paper, we focus on wind-induced climatic hazards (e.g., hurricane, tornadoes), since they pose the top resilience-related threat to distribution systems. As depicted in Fig. 1, the ROD problem is modeled as a two-stage stochastic decision process: (i) the planner makes ROD decisions, i.e., pole hardening, installing backup DGs and adding sectionalizers in the first stage; (ii) then the operational uncertainties are resolved during the hazards, which include (a) power demand, (b) line damage statuses, and (c) line repair costs; (iii) the operator makes the recourse decisions (i.e., DG re-dispatch,
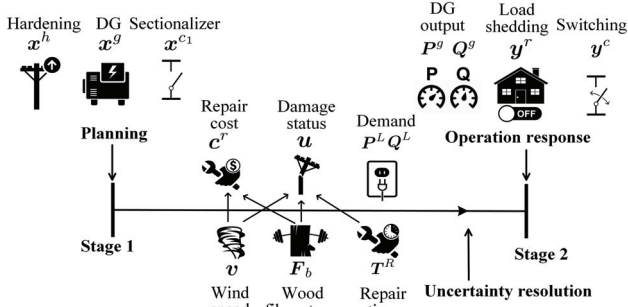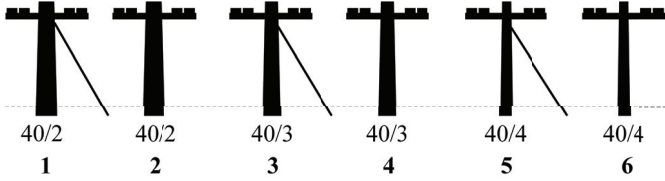
Fig. 1. Decision process for ROD problem.
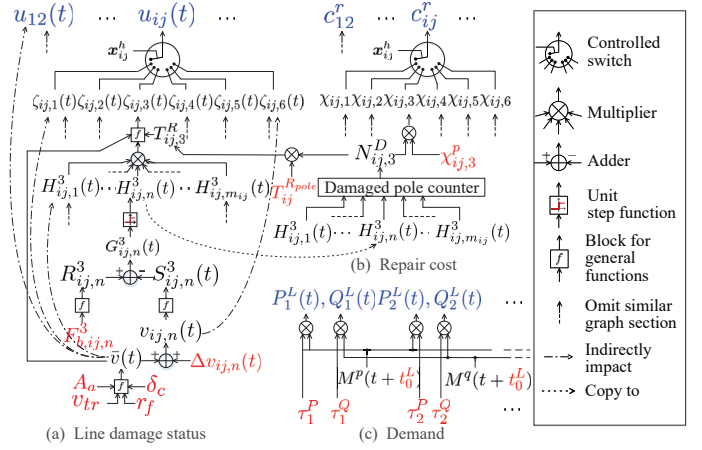

Fig. 2. Pole types.

Fig. 3. The structure of uncertainty space: independent observable random variables/processes (highlighted in red) + deterministic casual connections (parameterized by the first-stage decision).

load shedding, and reconfiguration) to minimize the operational cost in climatic hazards in the second stage. Notice that the line statuses are determined by wind speeds, pole strengths, and repair times, all of which are stochastic. In particular, pole strengths and repair times are decision-dependent.

A. The First Stage Decisions

The resilience of distribution systems can be effectively enhanced by (i) strengthening vulnerable components, (ii) increasing adequacy of power supply, and (iii) increasing topological flexibility. Accordingly, this paper considers the following resilience-enhancing methods: (a) upgrading pole classes, (b) adding transverse guys, (c) installing backup DGs, and (d) adding sectionalizers. Thus, the first-stage decisions are represented by a row vector $\boldsymbol{x} = \left[\boldsymbol{x}^h, \boldsymbol{x}^g, \boldsymbol{x}^{c_1}\right]$, which is explained as follows.

1) Hardening poles: For illustration, three commonly used pole types are considered: Southern Yellow Pine pole 40-2, 40-3, and 40-4, each with or without guying [15]. Thus, there are $2 \times 3 = 6$ pole types (see Fig. 2). For each line section, 6 binary decision variables are used to represent which pole type is used for this line: let $\boldsymbol{x}^h_{ij} = \left[x^h_{ij,1}, x^h_{ij,2}, x^h_{ij,3}, x^h_{ij,4}, x^h_{ij,5}, x^h_{ij,6}\right] \in \{\mathbf{1}, \mathbf{2}, \mathbf{3}, \mathbf{4}, \mathbf{5}, \mathbf{6}\}$ denote the selected pole type for line (i,j). For example, $\boldsymbol{x}^h_{ij} = \left[x^h_{ij,1}, x^h_{ij,2}, x^h_{ij,3}, x^h_{ij,4}, x^h_{ij,5}, x^h_{ij,6}\right] = \mathbf{1} = [1,0,0,0,0,0]$ indicates pole type 1 (40-2 with guys) is used. We have $\boldsymbol{x}^h = \left[\boldsymbol{x}^h_1, \boldsymbol{x}^h_2, \ldots, \boldsymbol{x}^h_{|\Omega_B|}\right] \in \{0,1\}^{6|\Omega_B|}$ denoting pole types and implying pole hardening decisions of all lines. The formulation can be easily extended to include more pole types.

2) Installing Backup DGs: This paper considers backup DGs that are dispatchable during hazards. Let $\boldsymbol{x}^g = \left[x^g_1, x^g_2, \ldots, x^g_{|\Omega_N|}\right] \in \{0,1\}^{|\Omega_N|}$ denote the DG deployment decisions, where a DG will be installed at node i if $x^g_i = 1$.

3) Adding sectionalizers: The automatic sectionalizers can be added at both ends of a line. They can be used to reroute the power flow, and isolate the faulted or damaged network sections. Let $\boldsymbol{x}^{c_1}_{ij} = \left[x^{c_1}_{ij,i}, x^{c_1}_{ij,j}\right] \in \{0,1\}^2$, where a

sectionalizer is added at the end i of line (i,j) if $x^{c_1}_{ij,i} = 1$, and a sectionalizer is deployed at the end j of line (i,j) if $x^{c_1}_{ij,j} = 1$. We have $\boldsymbol{x}^{c_1} = \left[\boldsymbol{x}^{c_1}_1, \boldsymbol{x}^{c_1}_2, \ldots, \boldsymbol{x}^{c_1}_{|\Omega_B|}\right] \in \{0,1\}^{2|\Omega_B|}$ denoting the decisions of deploying sectionalizers.

B. Uncertainty Modeling

The key challenge of uncertainty modeling in a ROD problem is the spatial-temporal correlations among ROD decisions, climatic hazard uncertainties, and system operations. Besides, the hazards and system operations are time-varying. It is challenging to model these uncertainties by formulating a high-dimensional joint distribution. Therefore, a hybrid of independent stochastic processes and deterministic causal structure is proposed as shown in Fig. 3. Based on this structure, we firstly sample independent random variables individually and then generate the correlated latent variables using the causal structure. Finally, three groups of random variables that have direct impacts on the evolution of the system operation state can be obtained (highlighted in blue): (a) line damage statuses $\boldsymbol{u}(t; \boldsymbol{x}^h) \in \{0,1\}^{|\Omega_B|}$ for $t \in \mathcal{T}_H$, where $\mathcal{T}_H$ is the time horizon set of a climatic hazard, and $|\mathcal{T}_H|$ equals the hazard duration plus the longest line repair time; (b) repair costs $\boldsymbol{c}^r \in \mathbb{R}_+^{|\Omega_B|}$; and (c) load demands $\boldsymbol{P}^L(t)$, $\boldsymbol{Q}^L(t)$, for $t \in \mathcal{T}_H$. We use $\xi = \left[\boldsymbol{u}, \boldsymbol{c}^r, \boldsymbol{P}^L, \boldsymbol{Q}^L\right] : \Omega \to \Omega_\mathcal{S}$ to denote the random variable associated to a scenario.

1) Line Damage Status: Notice that the first-stage decision variable $\boldsymbol{x}^h$ is a parameter in $\boldsymbol{u}(t; \boldsymbol{x}^h)$ as hardening poles reduces the probability of line damage. This raises the challenge of sampling the random variables, since the distribution of $\boldsymbol{u}(t)$ cannot be determined before the decision $\boldsymbol{x}^h$ is known. It is reasonable to assume that a line's damage status is related to its own pole type, i.e., $u_{ij}(t; \boldsymbol{x}^h) = u_{ij}(t; \boldsymbol{x}^h_{ij})$ for all $(i,j) \in \Omega_B, t \in \mathcal{T}_H$, and the number of possible values of $\boldsymbol{x}^h_{ij}$ is small (6 in this paper) compared to the number of possible values of $\boldsymbol{x}^h$ ($6^{|\Omega_B|}$). Thus, each $u_{ij}(t)$ can be sampled in advance for all possible values of $\boldsymbol{x}^h_{ij}$, which are $\zeta_{ij,1}(t), \ldots, \zeta_{ij,6}(t)$ in Fig. 3(a). We can regard them as different *versions* of $u_{ij}(t)$ in six "parallel universes", and only one of them will finally realize according to the value of $\boldsymbol{x}^h_{ij}$

in the ROD solution. This selection logic is represented by constraint (13) in Section III.

A line is damaged when at least one pole of the line section is damaged, and it remains damaged status until the repair is finished. We assume all the repair starts after the wind-induced hazard ends (the wind speed drops to a certain level). Take $\zeta_{ij,3}(t)$ in Fig. 3(a) as an example. Each version of $u_{ij}(t)$ is determined by whether any pole of line (i,j) can be damaged, i.e., $H^3_{ij,1}(t),\ldots,H^3_{ij,m_{ij}}(t)$ under this version, the wind speed trend $\bar{v}(t)$ (detailed later), and the repair time of line (i,j), i.e., $T^R_{ij,3}$. This paper assumes $T^R_{ij,k} = N^D_{ij,k} \cdot T^{R_{pole}}_{ij}$, where $N^D_{ij,k}$ is the total number of damaged poles of line (i,j) under version k, and $T^{R_{pole}}_{ij}$ is the repair time for a single pole. For all $(i,j) \in \Omega_B$, $T^{R_{pole}}_{ij}$ is a random variable with an independent identical Weibull distribution:

$$f_{T^{R_{pole}}_{ij}}(t)=\begin{cases}\frac{\beta_T}{\alpha_T}(\frac{t}{\alpha_T})^{\beta_T-1}\exp[-(\frac{t}{\alpha_T})^{\beta_T}] & \text{if } t\geqslant 0 \\ 0 & \text{otherwise,}\end{cases} \quad (1)$$

where $\beta_T = 10$ and $\alpha_T = 4$ [6]. $N^D_{ij,3}$ can be obtained given $H^3_{ij,1}(t),\ldots,H^3_{ij,m_{ij}}(t)$.

Fragility models have been used to determine whether a pole will be damaged by a hurricane, e.g., a fragility model that uses a log-normal distribution to express a pole's failure probability as a function of wind speed [7], [12]. It represents the probability that a pole will reach a defined limit state within a given period. But it cannot model the temporal correlation of damages or provide the exactly damaged time. In Fig. 3(a), a pole's status (damaged or functional) in each version is simulated at every time instant based on the structural limit state function $G(t)=R-S(t)$ in [16]. Here the scalar quantities R and $S(t)$ are functions of a number of more basic parameters corresponding to a reliability formulation of high dimension in the structural design of civil engineering. Take the n-th pole as an example, $H^3_{ij,n}(t)$ is determined by comparing the pole resistance under current version, i.e., $R^3_{ij,n}$, and the wind load under current version, i.e., $S^3_{ij,n}(t) : H^3_{ij,n}(t) = 0$ iff $R^3_{ij,n} \leqslant S^3_{ij,n}(t)$, which implies that the nth pole of line (i,j) can be damaged by the wind-induced hazard at time t under version 3; $H^3_{ij,n}(t) = 1$ iff $R^3_{ij,n} > S^3_{ij,n}(t)$. $R^3_{ij,n}$ captures the impact of pole types. The discrepancy among different poles of the same type is described by $F^3_{ij,n}$, which is modeled by a normal distribution with mean of 8000 psi and standard deviation of 1600 psi [17]. According to the pole type (which is 3 here), $S^3_{ij,n}(t)$ is a function of the time-varied wind speed that the nth pole of line (i,j) experiences (detailed in [16]). The wind speed can be decomposed into two components: the slow varying part $\bar{v}(t)$ (trend) and the fast varying part $\Delta v_{ij,n}(t)$ (volatility). Since the geographic range of a distribution system is usually much smaller compared to the areas being affected by a wind-induced hazard, it is assumed: (i) $\bar{v}(t)$ (detailed in [18]) is shared by all versions, all lines and all poles; and (ii) $\Delta v_{ij,n}(t)$ follows an independent and identical normal distribution for all poles of all lines [18]. The dot-dashed lines in Fig. 3(a) illustrate these assumptions.

2) Repair cost: Similarly, $\chi_{ij,1},\ldots,\chi_{ij,6}$ represent the 6 versions of the repair cost of line (i,j), for the 6 pole types. Take version 3 as an example [see Fig. 3(b)], we assume

$\chi_{ij,3} = N^D_{ij,3} \cdot \chi^p_{ij,3}$, where $\chi^p_{ij,3}$ is the repair cost for a single pole in the current version, which is assumed to be constant.

3) Demand: The power demand of load $i \in \Omega_L$ is assumed to be the product of a random multiplier, τ^P_i or τ^Q_i, and the hourly normalized load profile. For the multipliers, assume

$$\tau^P_i \sim N(\overline{P}_i, (0.02\overline{P}_i)^2), \forall i \in \Omega_L \quad (2)$$

$$\tau^Q_i \sim N(\overline{Q}_i, (0.02\overline{Q}_i)^2), \forall i \in \Omega_L \quad (3)$$

are independent for all i, where $\overline{P}_i$ and $\overline{Q}_i$ represent the mean values of daily peak active and reactive power of load i over a year, respectively. We use $M^p(t)$ and $M^q(t)$ to make load profile shapes change with time. In this paper, all loads are assumed to share the same $M^p(t)$ and $M^q(t)$. Since the wind-induced hazard could happen at any time, let assume a uniformly distributed time offset, t^L_0, for the load profiles. Thus, it will have

$$P^L_i(t) = \tau^P_i \cdot M^p(t + t^L_0), \forall i \in \Omega_L, t \in \mathcal{T}_H \quad (4)$$

$$Q^L_i(t) = \tau^Q_i \cdot M^q(t + t^L_0), \forall i \in \Omega_L, t \in \mathcal{T}_H. \quad (5)$$

Notice that all variables at the source nodes in Fig. 3 (highlighted in red) are independent. Thus, they can be independently sampled, which can be performed in parallel with a small computational burden.

C. The Second Stage Decisions

After the uncertainty is resolved, the system operator makes the recourse decisions to minimize operation costs. The second-stage operation decisions can be represented by a vector $\boldsymbol{y}^{R,s} = [\boldsymbol{P}^{g,s}, \boldsymbol{Q}^{g,s}, \boldsymbol{y}^{c,s}, \boldsymbol{y}^{r,s}]$, where $\boldsymbol{P}^s_g$ and $\boldsymbol{Q}^s_g \in \mathbb{R}^{|\mathcal{T}_H|\times|\Omega_N|}_+$ denote the active and reactive power output of backup DGs for $t \in \mathcal{T}_H$; $\boldsymbol{y}^{c,s} \in \{0,1\}^{|\mathcal{T}_H|\times 2|\Omega_B|}$ denotes the status of all sectionalizers for $t \in \mathcal{T}_H$; $\boldsymbol{y}^{r,s} \in \mathbb{R}^{|\mathcal{T}_H|\times|\Omega_L|}_+$ denotes the load shedding ratios of all loads for all $t \in \mathcal{T}_H$.

III. A TWO-STAGE STOCHASTIC OPTIMIZATION FORMULATION AND ALGORITHM SOLUTION

In this paper, a two-stage stochastic mixed-integer ROD formulation is developed. The objective of the first stage is to minimize the costs of hardening lines, installing backup DGs, adding sectionalizers, and the expected cost of the second stage. The second stage is to minimize the costs of loss of load, DG operation and damage repair. The first-stage problem is a linear integer program, and the second stage is a mixed-integer linear program.

A. The First-Stage Problem

$$\min \sum_{(i,j)\in\Omega_B}\sum_{k\in\Omega_K}c_{ij,k}x^h_{ij,k}+\sum_{i\in\Omega_N}c^g_i x^g_i + \sum_{(i,j)\in\Omega_B}c^c_{ij}(x^{c_1}_{ij,i}+x^{c_1}_{ij,j})+\mathcal{Q}(x) \quad (6)$$

$$s.t. \sum_{k\in\Omega_K} x^h_{ij,k} = 1, \forall(i,j) \in \Omega_B \quad (7)$$

$$\sum_{i\in\Omega_N} x^g_i \leqslant N_G \quad (8)$$

$$x^{c_0}_{ij,n} + x^{c_1}_{ij,n} = x^c_{ij,n}, \forall(i,j) \in \Omega_B, n \in \{i,j\} \quad (9)$$

$$x_{ij,k}^h, x_{ij,n}^{c_1}, x_{ij,n}^c, x_i^g \in \{0,1\}, \forall i \in \Omega_N, (i,j) \in \Omega_B, \\ k \in \Omega_H, n \in \{i,j\} \tag{10}$$

$$\text{where} \quad \mathcal{Q}(x) = w_H \cdot \mathbb{E}_{\boldsymbol{\xi}} \phi(x, \boldsymbol{\xi}) \cong w_H \cdot \sum_{s \in \mathcal{S}} p_r(s) \phi(x, s) \tag{11}$$

In the objective function, $c_{ij,k}$ represents the hardening cost of line (i,j) with k-th pole type, which is also related to the original pole type before hardening. If the original pole type at line (i,j) is assumed to be **3**, then $c_{ij,3} = 0$. For example, $c_{ij,2}$ equals the cost of replacing all poles associated with line section (i,j) to pole type 2, and $c_{ij,1}$ equals the cost of upgrading all poles at line (i,j) to pole type 2 with pole guying. Constraint (7) indicates that only one hardening strategy can be selected for each line. Constraint (8) restricts the number of DGs that can be installed. $x_{ij,n}^c$ in constraint (9) represents whether line (i,j) has a switch or not at the end of n, which is used in the second-stage problem. The second-stage expected cost is given by equation (11), where w_H is the total number of the wind-induced hazards occurring in a year and $p_r(s)$ is the scenario sample probability, which equals $\frac{1}{|\mathcal{S}|}$.

B. The Second-Stage Problem

In the second stage, the sectionalizers isolate damaged lines with the minimal service interruption. Since the distribution network is assumed to be radial in this paper, the opening of sectionalizers can separate the network into a few *islands*. The "healthy islands", i.e., islands without damaged lines and with power supply from the substation and/or DGs, are supposed to operate as stand-alone microgrids; the "unhealthy islands" will be de-energized until they are gradually recovered in the repair stage. During the repair stage, if a part of the de-energized island becomes healthy and there exists a breaker or sectionalizer that can isolate it from the remaining unhealthy part, this part will be prioritized in the repair, and operate as a MG. Finally, when all damaged lines are repaired, the system will return to normal operating condition. For each healthy island, DG dispatching and load shedding will be used to meet the load demand as much as possible. It is necessary to develop a mathematic formulation that can model self-healing operations mentioned above. For this purpose, there are two main challenges: (i) the sectionalizers and breakers only exist in certain line sections, which poses the challenge to isolate the damaged part with the minimum customer interruptions; and (ii) the energized networks should keep radial topologies to reduce potential operation issues, and facilitate the system to return to the normal operation topology when all damaged lines are repaired.

1) Modeling strategy: A novel modeling method is proposed to meet the challenge (i). The idea is to add a *fictitious fault* at a damaged line [19]. A line damage will not necessarily lead to a fault, but the damaged line should be isolated as if it was faulted. Therefore, the system model is modified by inserting a virtual node in the middle of each line, then a symmetric ground fault at the virtual node is applied if the line is damaged. The virtual node is also included in power flow constraints. The second key modification is to set the bus voltage magnitude feasible region to be $\{0\} \cup [V^{\min}, V^{\max}]$ in (26), where $[V^{\min}, V^{\max}]$ is the safe range, i.e., $0.9 \sim 1.1 p.u.$. If

the voltage magnitude of a faulted line is within $0.9 \sim 1.1 p.u$ and there is no switch on that line, it causes a large fault current, which violates the power flow constraints (19)-(20). Consequently, the voltage magnitude at the two ends of the faulted line is forced to be zero. This fictitious faulting logic propagates to the rest of the network until a switch can break it. It results in a de-energized island with zero voltages, which is formed by all line sections that are directly connected to the faulted line without switches in between. In this case, there is no power flow in the island, given constraint (23). Constraint (29) disconnects the DGs on a faulted bus. The load shedding is minimized in the objective (12), which encourages all sectionalizers to block the fault propagation, and maximizes the load service in the healthy islands.

To solve the challenge (ii), the network is represented as a forest. The radiality constraint for a forest can be constructed according to a theorem in graph theory [20]: A forest of N nodes has exactly $N - N_c$ edges, where N_c is the number of connected network components. Thus, the radiality constraint is satisfied *iff* the number of active branches equals $N - N_c$. The calculation of N_c is based on the fact that when power flow equations are satisfied, the voltage angles of a connected network component (healthy island) have exactly one degree of freedom counted. Hence, the number of components can be calculated by the degree of freedom of voltage angles. To obtain this degree of freedom, a virtual DC optimal power flow (VDCOPF) subproblem is formulated. The optimal solution of this subproblem satisfies that the virtual loads in the same energized island are nearly equally distributed at active nodes and each energized island has and only has an active node with zero angle. Since the continuous VDCOPF subproblem has a positive definite quadratic objective and linear constraints, it can be equivalently replaced by the corresponding Karush-Kuhn-Tucker (KKT) condition in MILP form. The dual variable of voltage angle in KKT condition is used as the indicator of zero angle. The formulation of the above modeling strategies is detailed below.

Let Ω_{B_F} denote the line set considering virtual nodes (each line is divided into two parts by its virtual node), Ω_F denotes the set of virtual nodes, and $\Omega_{N_F} = \Omega_N \cup \Omega_F$. For $(i,j) \in \Omega_{B_F}$, i is assumed to represent the original node, where $i \in \Omega_N$, and j is assumed to represent the virtual node, where $j \in \Omega_F$. The power injection direction at node i is assumed to be flowing out, and the power injection direction at node j is flowing in.

2) Least-cost objective: The objective (12) is to minimize the total cost of the loss of load, DG operation, repair, and the weighted penalty cost of voltage angles and the relaxation of line flows given a specific scenario s and fixed first-stage decisions.

$$\phi(\boldsymbol{x}, s) = \min \sum_{i \in \Omega_N} \sum_{t \in \mathcal{T}_H^s} c_i^L y_{i,t}^{r,s} P_{i,t}^{L,s} \Delta t + \sum_{i \in \Omega_N} \sum_{t \in \mathcal{T}_H^s} c_i^o P_{i,t}^{g,s} \Delta t \\ + \sum_{(i,j) \in \Omega_B} c_{ij}^{r,s} \tag{12}$$

3) Line damage status constraint:

$$u_{ij,t}^s = \sum_{k \in \Omega_K} x_{ij,k}^h \zeta_{ij,k,t}^s, \forall (i,j) \in \Omega_B, t \in \mathcal{T}_H^s \tag{13}$$

As mentioned in Section II-B1, we only need to sample $\zeta^s_{ij,k,t}$ for all (i,j) independently in the phase of scenario generation. The line damage status $u^s_{ij,t}$ will be decided by $x^h_{ij,k}$ and $\zeta^s_{ij,k,t}$.

4) Line repair cost constraint:

$$c^{r,s}_{ij} = \sum_{k \in \Omega_K} x^h_{ij,k} \chi^s_{ij,k}, \forall (i,j) \in \Omega_B \qquad (14)$$

As mentioned in Section II-B2, the line repair cost $c^{r,s}_{ij}$ can be decided by $x^h_{ij,k}$ and $\chi^s_{ij,k}$.

5) Line's on-off status constraints: A line's on-off status is controlled by two decision variables, x^c_{ij}, and $y^{c,s}_{ij,t}$, $\forall (i,j) \in \Omega_{B_F}$. Here $x^c_{ij}, \forall (i,j) \in \Omega_{B_F}$ is the same expression of $x^c_{ij,n}, \forall n \in \{i,j\}, (i,j) \in \Omega_B$. It is beneficial to introduce a new decision variable $w^{o,s}_{ij,t}, \forall (i,j) \in \Omega_{B_F}, t \in \mathcal{T}^s_H$ to represent the line's on-off status (e.g. $w^{o,s}_{ij,t} = 1$ means line (i,j) is on at time t). Table I lists the desired values of $w^{o,s}_{ij,t}$ given all possible combinations of x^c_{ij} and $y^{c,s}_{ij,t}$.

TABLE I
EVALUATION OF THE ON-OFF STATUS VARIABLE

x^c_{ij}	$y^{c,s}_{ij,t}$	$w^{o,s}_{ij,t}$	x^c_{ij}	$y^{c,s}_{ij,t}$	$w^{o,s}_{ij,t}$
0	0	1	1	0	1
0	1	N/A	1	1	0

*N/A: the case should be infeasible.

This evaluation table can be formulated by

$$y^{c,s}_{ij,t} \leqslant x^c_{ij}, \forall (i,j) \in \Omega_{B_F}, t \in \mathcal{T}^s_H \qquad (15)$$

$$x^c_{ij} + y^{c,s}_{ij,t} + 2w^{o,s}_{ij,t} \geqslant 2, \forall (i,j) \in \Omega_{B_F}, t \in \mathcal{T}^s_H \qquad (16)$$

$$w^{o,s}_{ij,t} + y^{c,s}_{ij,t} \leqslant 1, \forall (i,j) \in \Omega_{B_F}, t \in \mathcal{T}^s_H \qquad (17)$$

$$y^{c,s}_{ij,t}, w^{o,s}_{ij,t} \in \{0,1\}, \forall (i,j) \in \Omega_{B_F}, t \in \mathcal{T}^s_H \qquad (18)$$

Constraint (15) indicates that closing a sectionalizer is feasible only if it exits. If a line has no sectionalizer or breaker on it ($x^c_{ij} = y^c_{ij,t} = 0$), the line's status will be on as shown in (16); if a line has a sectionalizer ($x^c_{ij} = 1$), the line's status will be controlled by $y^c_{ij,t}$ in (17).

6) Line flow limits:

$$-w^{o,s}_{ij,t}P^{\max}_{ij} \leqslant P^s_{ij,t} \leqslant w^{o,s}_{ij,t}P^{\max}_{ij}, \forall (i,j) \in \Omega_{B_F}, t \in \mathcal{T}^s_H \quad (19)$$

$$-w^{o,s}_{ij,t}Q^{\max}_{ij} \leqslant Q^s_{ij,t} \leqslant w^{o,s}_{ij,t}Q^{\max}_{ij}, \forall (i,j) \in \Omega_{B_F}, t \in \mathcal{T}^s_H \quad (20)$$

Constraints (19)-(20) approximate the line flow limits. If $w^{o,s}_{ij,t} = 0$, the state of line (i,j) is off, and there is no power flow through i node to j node.

7) Linearized DistFlow equations: Constraints (21)-(23) represent the linearized DistFlow equations, which have been widely used in distribution systems [9], [11], [21].

$$\sum_{\{j|(i,j) \in \Omega_{B_F}\}} P^s_{ij,t} = P^{g,s}_{i,t} - (1-y^{r,s}_{i,t})P^L_{i,t} - \varepsilon_1 V^s_{i,t}, \forall i \in \Omega_N, t \in \mathcal{T}^s_H$$

$$(21)$$

$$\sum_{\{j|(i,j) \in \Omega_{B_F}\}} Q^s_{ij,t} = Q^{g,s}_{i,t} - (1-y^{r,s}_{i,t})Q^L_{i,t}, \forall i \in \Omega_N, t \in \mathcal{T}^s_H \quad (22)$$

$$V^s_{i,t} - \frac{R^e_{ij}P^s_{ij,t} + X^e_{ij}Q^s_{ij,t}}{V_0} - (1-w^{o,s}_{ij,t})M_1 \leqslant V^s_{j,t} \leqslant V^s_{i,t}$$
$$- \frac{R^e_{ij}P^s_{ij,t} + X^e_{ij}Q^s_{ij,t}}{V_0} + (1-w^{o,s}_{ij,t})M_1, \forall i \in \Omega_{N_F}, t \in \mathcal{T}^s_H$$
$$(23)$$

Equations (21)-(22) represent power balance at each node. Constraint (23) indicates the relationship of voltage magnitudes of neighboring buses. A big M approach is used to decouple voltages of two buses connected by a line that is off. The network connectivity, which is affected by line on-off status, is represented by constraints (19)-(23).

8) Virtual node power injection constraints:

$$-u^s_{ij,t}M_2 \leqslant \sum_{k \in \{i,j\}} P^s_{kf_{ij},t} + \varepsilon_1 \cdot V^s_{i,t} \leqslant u^s_{ij,t}M_2, \forall (i,j) \in \Omega_B,$$
$$f_{ij} \in \Omega_{N_F}, t \in \mathcal{T}^s_H$$
$$(24)$$

$$-u^s_{ij,t}M_2 \leqslant \sum_{k \in \{i,j\}} Q^s_{kf_{ij},t} \leqslant u^s_{ij,t}M_2, \forall (i,j) \in \Omega_B, f_{ij} \in \Omega_{N_F}, t \in \mathcal{T}^s_H$$
$$(25)$$

Constraint (24)-(25) indicate that if line (i,j) is not damaged, the power injection at the virtual node f_{ij} is zero; if line (i,j) is damaged, constraint (24)-(25) is canceled off, and if its voltage is within the normal range, it will cause a large short current.

9) Voltage magnitude limits:

$$w^{m,s}_{i,t}V^{\min}_i \leqslant V^s_{i,t} \leqslant w^{m,s}_{i,t}V^{\max}_i, \forall i \in \Omega_{N_F}, t \in \mathcal{T}^s_H \quad (26)$$

$$u^s_{ij,t} + w^{m,s}_{f_{ij},t} \leqslant 1, \forall (i,j) \in \Omega_B, f_{ij} \in \Omega_F, t \in \mathcal{T}^s_H \quad (27)$$

$$w^{m,s}_{i,t} \in \{0,1\}, \forall i \in \Omega_{N_F}, t \in \mathcal{T}^s_H \quad (28)$$

The auxiliary binary variable $w^{m,s}_{i,t}$ in (26) is introduced to give different restrictions on the voltage magnitude: if $w^{m,s}_{i,t} = 1$, the voltage magnitude will be restricted to be within the safe range; if $w^{m,s}_{i,t} = 0$, then $V^s_{i,t} = 0$. When line (i,j) is damaged, constraints (26)-(27) are used to force the voltage magnitude at the virtual node to be zero ($V_{f_{ij},t} = 0$).

10) Load shedding ratio limit:

$$1 - w^{m,s}_{i,t} \leqslant y^{r,s}_{i,t} \leqslant 1, \forall i \in \Omega_N, t \in \mathcal{T}^s_H \quad (29)$$

The load shedding ratio limit is shown in constraint (29). If the voltage magnitude of a node is zero, load shedding ratio at that node will be 1. In the objective function, the cost of load shedding is used as a severity index for a climatic hazard.

11) DG capacity limits and operation status:

$$0 \leqslant P^{g,s}_{i,t} \leqslant x^g_i P^{g,\max}_i, \forall i \in \Omega_N, t \in \mathcal{T}^s_H \quad (30)$$

$$0 \leqslant Q^{g,s}_{i,t} \leqslant x^g_i Q^{g,\max}_i, \forall i \in \Omega_N, t \in \mathcal{T}^s_H \quad (31)$$

Constraints (30)-(31) represent the generation capacity limits of DG at node i if it has been installed in the first stage.

12) Radiality constraints:

$$\sum_{(i,j) \in \Omega_{B_F}} w^{b,s}_{ij,t} = \sum_{i \in \Omega_{N_F}} w^{m,s}_{i,t} - \sum_{i \in \Omega_{N_F}} w^{a,s}_{i,t} \quad (32)$$

$$w^{o,s}_{ij,t} + w^{m,s}_{i,t} - 1 \leqslant w^{b,s}_{ij,t} \leqslant 0.5w^{o,s}_{ij,t} + 0.5w^{m,s}_{i,t}$$
$$\forall i \in \Omega_{N_F}, (i,j) \in \Omega_{B_F}, t \in \mathcal{T}^s_H$$
$$(33)$$

$$w^{a,s}_{i,t}, w^{b,s}_{ij,t} \in \{0,1\}, \forall i \in \Omega_{N_F}, (i,j) \in \Omega_{B_F}, t \in \mathcal{T}^s_H \quad (34)$$

The radiality constraint can be expressed by (32), where the number of active branches equals the total number of active nodes minus the number of active nodes with zero angles [19]. Here a new binary variable $w_{ij,t}^{b,s}$ is introduced to represent the active branch since $w_{ij,t}^{o,s}$ cannot fully indicate whether that line is energized. For example, if line (i,j) is damaged, its connected lines without a sectionalizer or breaker will also be de-energized although their line statuses are on. Constraint (33) indicates whether line (i,j) is an active line, is decided by two decision variables, $w_{ij,t}^{o,s}$ and $w_{i,t}^{m,s}$. $w_{i,t}^{m,s} = 1$ can be regarded as an indicator of active node. If line's status is on ($w_{ij,t}^{o,s} = 1$) and node i is an active node ($w_{i,t}^{m,s} = 1$), it must be an active branch. Since a small constant current load ($\varepsilon_1 \cdot V_{i,t}^s$) in constraint (21) and (24) can impose all the nodes' voltage magnitude in the de-energized but no fault areas be zero.

13) The minimality condition of VDCOPF subproblem:

$$
\begin{aligned}
\left(\mathcal{P}_{L,t}^{s,\star}, \mathcal{P}_{l,t}^{s,\star}, \theta_t^{s,\star}\right) = &\underset{\mathcal{P}_{L,t}^s, \mathcal{P}_{l,t}^s, \theta_t^s}{\arg\min} \left\{ \sum_{i \in \Omega_{N_F}} \left(\theta_{i,t}^s + \frac{\alpha_L}{2}(\mathcal{P}_{L,i,t}^s)^2\right) \right. \\
&\left. a: -\left(1 - w_{ij,t}^{o,s}\right)M_3 \leqslant \mathcal{P}_{ij,t}^s - S_0 B_{ij}' \left(\theta_{i,t}^s - \theta_{j,t}^s\right) \right. \\
&\qquad\qquad \leqslant \left(1 - w_{ij,t}^{o,s}\right)M_3, \forall(i,j) \in \Omega_{B_F} \\
\text{s.t.} \quad &\left. b: -w_{ij,t}^{o,s}M_3 \leqslant \mathcal{P}_{ij,t}^s \leqslant w_{ij,t}^{o,s}M_3, \forall(i,j) \in \Omega_{B_F} \right. \\
&\left. c: \sum_{\{j|(i,j)\in\Omega_{B_F}\}} \mathcal{P}_{ij,t}^s - P_{i,t}^{g,s} + \mathcal{P}_{L,i,t}^s = 0, \forall i \in \Omega_{N_F} \right. \\
&\left. d: -\theta_{i,t}^s \leq 0, \quad \forall i \in \Omega_{N_F} \right. \\
&\left. e: -\mathcal{P}_{L,i,t}^s \leq 0, \quad \forall i \in \Omega_{N_F} \right\} \\
&\qquad\qquad \forall t \in \mathcal{T}_H^s
\end{aligned}
$$

$$(35)$$

VDCOPF subproblem is modeled to realize that a connected network component (healthy MG) has one and only one degree of freedom of voltage angle under the condition of full DC power flow equations. The non-negative constraint on voltage angles and the corresponding summation penalty function in the objective force the minimum value of voltage angles in active components to be zero. Meanwhile, minimizing the sum of squares of virtual loads in the objective encourages the virtual loads to be equally distributed on active nodes in healthy MGs. Such a load distribution plus the standardized B_{ij}' (with random noise) ensure the bus of minimum angle (i.e., zero angle) is unique for each active component. In this way, the number of zero angles in active components is equal to the number of healthy MGs. Notice that the DC power flow equations (35).a-c are isolated from the actually power flow constraints, i.e., the DisFlow equations in (21)-(23), by the subproblem. Only line on-off status and DG output are passed to the VDC OFF subproblem, as to avoid the potential conflicts between two suits of power flow equations.

Equation (35) can be equivalently replaced by its KKT condition:

Primal feasibility

$$
-\left(1-w_{ij,t}^{o,s}\right)M_3 \leqslant \mathcal{P}_{ij,t}^{s,\star} - S_0 B_{ij}' \left(\theta_{i,t}^{s,\star} - \theta_{j,t}^{s,\star}\right) \leqslant \left(1-w_{ij,t}^{o,s}\right)M_3,
$$
$$
\forall(i,j) \in \Omega_{B_F}, t \in \mathcal{T}_H^s
$$
$$
-w_{ij,t}^{o,s}M_3 \leqslant \mathcal{P}_{ij,t}^{s,\star} \leqslant w_{ij,t}^{o,s}M_3, \forall(i,j) \in \Omega_{B_F}, t \in \mathcal{T}_H^s
$$
$$
\sum_{\{j|(i,j)\in\Omega_{B_F}\}} \mathcal{P}_{ij,t}^{s,\star} - P_{i,t}^{g,s} + \mathcal{P}_{L,i,t}^{s,\star} = 0, \forall i \in \Omega_{N_F}, t \in \mathcal{T}_H^s
$$

$$(36)$$

Stationarity

$$
\partial\mathcal{L}/\partial\mathcal{P}_{L,i,t}^{s,\star} : \alpha_L \mathcal{P}_{L,i}^{s,\star} + \lambda_{c,i,t}^s - \mu_{e,i,t}^s = 0, \forall i \in \Omega_{N_F}, t \in \mathcal{T}_H^s
$$
$$
\partial\mathcal{L}/\partial\mathcal{P}_{ij,t}^{s,\star} : -\lambda_{a,ij,t}^s + \lambda_{b,ij,t}^s + \lambda_{c,i,t}^s - \lambda_{c,j,t}^s = 0,
$$
$$
\forall(i,j) \in \Omega_{B_F}, t \in \mathcal{T}_H^s
$$
$$
\partial\mathcal{L}/\partial\theta_{i,t}^{s,\star} : \sum_{\{j|(i,j)\in\Omega_{B_F}\}} \lambda_{a,ij,t}^s B_{ij} S_0 + 1 - \mu_{d,i,t}^s = 0,
$$
$$
\forall i \in \Omega_{N_F}, t \in \mathcal{T}_H^s
$$

$$(37)$$

Complementary slackness and dual feasibility

$$
0 \leqslant \mu_{d,i,t}^s \perp \theta_{i,t}^{s,\star} \geqslant 0, \qquad \forall i \in \Omega_{N_F}, t \in \mathcal{T}_H^s
$$
$$
0 \leqslant \mu_{e,i,t}^s \perp \mathcal{P}_{L,i,t}^{s,\star} \geqslant 0, \quad \forall(i,j) \in \Omega_{N_F}, t \in \mathcal{T}_H^s
$$

$$(38)$$

On-off line status

$$
-\left(1-w_{ij,t}^{o,s}\right)M_4 \leqslant \lambda_{a,ij,t}^s \leqslant \left(1-w_{ij,t}^{o,s}\right)M_4, \forall i \in \Omega_{N_F}, t \in \mathcal{T}_H^s
$$
$$
-w_{ij,t}^{o,s}M_4 \leqslant \lambda_{b,ij,t}^s \leqslant w_{ij,t}^{o,s}M_4, \qquad \forall i \in \Omega_{N_F}, t \in \mathcal{T}_H^s
$$

$$(39)$$

14) Zero angle indicator constraints:

$$
w_{i,t}^{a,s} - 1 \leqslant \frac{1}{2|\Omega_{N_F}|}(\mu_{d,i,t}^s - 1 + \varepsilon_3) \leqslant w_{i,t}^{a,s}, \forall i \in \Omega_N, t \in \mathcal{T}_H^s
$$

$$(40)$$

Constraint (40) imposes $w_{i,t}^{a,s} = 1$ if $\mu_{d,i,t}^s > 1$, as $\mu_{d,i,t}^s$ has strong duality on $\theta_{i,t}^s$. If node i has zero angle ($\theta_{i,t}^s = 0$) in the healthy and active MG, its corresponding shadow price $\mu_{d,i,t}^s$ must be larger than 1 when each component has at least 2 buses (indicated by the coefficients of α_L in the objective).

C. A Compact Notation Form of ROD Model

For brevity, the proposed ROD model is written in a compact notation form. The first-stage problem is expressed as

$$
\min_{\boldsymbol{x}} \quad \left\{\boldsymbol{c}^\top \boldsymbol{x} + \mathcal{Q}(\boldsymbol{x}) : \boldsymbol{A}\boldsymbol{x} = \boldsymbol{b}\right\} \tag{41}
$$

where the vector $\boldsymbol{c}$ represents the cost for ROD methods; $\mathcal{Q}(\boldsymbol{x}) = \sum_{s \in \mathcal{S}} p_r(s)\phi(\boldsymbol{x}, s)$ is the recourse function of the second stage, which computes the expected value of taking decision $\boldsymbol{x}$. (41) is a vector form representation of first-stage constraints (7)-(9), where inequality constraints can be handled by the introduction of appropriate slack variables. The second stage value function $\phi(\boldsymbol{x}, s)$ is defined as follows:

$$
\min \quad \left\{\boldsymbol{q}(s)^\top \boldsymbol{y}^R : \boldsymbol{T}(s)\boldsymbol{x} + \boldsymbol{W}(s)\boldsymbol{y}^R = \boldsymbol{h}(s)\right\} \tag{42}
$$

The objective function in (42) is a compact expression of the objective function (12). Constraints (13)-(34) and (36)-(40) of the second-stage problem are written as an equality constraint in (42) by introducing appropriate slack variables for those inequality constraints.

D. Dual Decomposition Algorithm

The simplest approach to solve (6)-(31) is to apply a standard MIP solver, e.g., CPLEX, to directly solve its extensive form (EF). However, there is a computational challenge for solving the EFs of large-scale ROD problems by MIP solvers. Since both first and second stages contain integer variables, scenario-based decomposition methods, such as progressive hedging and dual decomposition (DD) have better performance than stage-based methods, such as integer L-shaped method, since they can reduce the computational difficulty

by decomposing the problem into scenario-based subproblems and solving subproblems in parallel [22]. Although the PH algorithm can find high-quality approximate solutions, it cannot guarantee optimality convergence [23]. We present a customized DD algorithm combined with branch-and-bound to obtain the optimal solutions of ROD problems.

The main idea of DD algorithm is to obtain lower bounds from Lagrangian dual by relaxing non-anticipativity constraints and using branch-and-bound to re-establish non-anticipativity [23]. Before we give the pseudocode of the proposed algorithm, it is better to explain the procedure of obtaining the best lower bound from Lagrangian dual, which will be used in the algorithm.

The deterministic equivalent of ROD problem can be written:

$$z = \min \left\{ \boldsymbol{c}^\top \boldsymbol{x} + \sum_{s \in S} p_r(s) \boldsymbol{q}^\top \boldsymbol{y}^{R,s} : (\boldsymbol{x}, \boldsymbol{y}^{R,s}) \in \boldsymbol{K}^s, \forall s \in S \right\} \tag{43}$$

where $\boldsymbol{K}^s = \{(\boldsymbol{x}, \boldsymbol{y}^{R,s}) : \boldsymbol{A}\boldsymbol{x} = \boldsymbol{b}, \boldsymbol{T}(s)\boldsymbol{x} + \boldsymbol{W}(s)\boldsymbol{y}^{R,s} = \boldsymbol{h}(s), \boldsymbol{x} \in \{0,1\}, \boldsymbol{y}^{R,s} = (\boldsymbol{y}_B^s, \boldsymbol{y}_C^s), \boldsymbol{y}_B^s \in \{0,1\}, \boldsymbol{y}_C^s \geqslant 0\}, \forall s \in \mathcal{S}$. Eq (43) is a large-scale deterministic MILP with a block-angular structure, which can lead decomposition methods to split it into more manageable scenario-based subproblems. To induce a scenario-based decomposable structure, the copies $\boldsymbol{x}^s, s \in \mathcal{S}$ of the first-stage variables $\boldsymbol{x}$ are introduced to create the following reformulation of (43):

$$\min \quad \left\{ \sum_{s \in S} p_r(s)(\boldsymbol{c}^\top \boldsymbol{x}^s + \boldsymbol{q}^\top \boldsymbol{y}^{R,s}) : \boldsymbol{x}^1 = \cdots = \boldsymbol{x}^{|S|}, \right.$$
$$\left. (\boldsymbol{x}^s, \boldsymbol{y}^{R,s}) \in \boldsymbol{K}^s, \forall s \in S \right\} \tag{44}$$

where $\boldsymbol{x}^1 = \cdots = \boldsymbol{x}^{|S|} = \overline{\boldsymbol{x}}$ represents the non-anticipativity constraint, which forces the first-stage decision not to be dependent on scenarios. The problem (44) can be decomposed when the non-anticipativity constraint is relaxed.

The Lagrangian relaxation with respect to the non-anticipativity constraint is the problem of finding $\boldsymbol{x}^s, \boldsymbol{y}^{R,s}, \forall s \in S$, such that

$$L(\boldsymbol{\mu}) = \min \left\{ \sum_{s \in S} \left[p_r(s)(\boldsymbol{c}^\top \boldsymbol{x}^s + \boldsymbol{q}^\top \boldsymbol{y}^{R,s}) + \boldsymbol{\mu}^s(\boldsymbol{x}^s - \overline{\boldsymbol{x}}) \right] : \right.$$
$$\left. (\boldsymbol{x}^s, \boldsymbol{y}^{R,s}) \in \boldsymbol{K}^s \right\} \tag{45}$$

with the condition $\sum_{s \in \mathcal{S}} \boldsymbol{\mu}^s = 0$ required for boundness of the Lagrangian. Here $\boldsymbol{\mu} = (\boldsymbol{\mu}^1, \cdots, \boldsymbol{\mu}^{|S|})$ is the vector of multipliers of the relaxed constraints $\boldsymbol{x}^s = \overline{\boldsymbol{x}}, \forall s \in S$.

The Lagrangian dual function in (45) can be separated into

$$L(\boldsymbol{\mu}) = \sum_{s \in \mathcal{S}} L_s(\boldsymbol{\mu}^s) \tag{46}$$

where $L_s(\boldsymbol{\mu}^s) = \min_{\boldsymbol{x}^s, \boldsymbol{y}^{R,s}} \{ p_r(s)(\boldsymbol{c}^\top \boldsymbol{x}^s + \boldsymbol{q}^\top \boldsymbol{y}^{R,s}) + \boldsymbol{\mu}^s \boldsymbol{x}^s :$
$$(\boldsymbol{x}^s, \boldsymbol{y}^{R,s}) \in \boldsymbol{K}^s \}, \forall s \in S \tag{47}$$

The Lagrangian dual of Eq. (44) then becomes the problem of finding the best lower bound:

$$z_{LD} = \max_{\boldsymbol{\mu}} \left\{ \sum_{s \in \mathcal{S}} L_s(\boldsymbol{\mu}^s) : \sum_{s \in \mathcal{S}} \boldsymbol{\mu}^s = 0 \right\} \tag{48}$$

The Lagrangian dual (48) is a convex non-smooth program and can be solved using subgradient methods.

According to Theorem 6.2 in [24], p. 327, we can get

$$z_{LD} = \min \left\{ \sum_{s \in S} p_r(s)(\boldsymbol{c}^\top \boldsymbol{x}^s + \boldsymbol{q}^\top \boldsymbol{y}^{R,s}) : \boldsymbol{x}^1 = \cdots = \boldsymbol{x}^{|S|}, \right.$$
$$\left. (\boldsymbol{x}, \boldsymbol{y}^R) \in \mathrm{conv} \times_{j=1}^{|S|} \boldsymbol{K}^s, \forall s \in S \right\} \tag{49}$$

As the fact that $\mathrm{conv} \times_{j=1}^{|S|} \boldsymbol{K}^s = \times_{j=1}^{|S|} \mathrm{conv} \boldsymbol{K}^s$, the optimal value z_{LD}^* of the Lagrangian dual (48) equals the optimal value of the linear program (50)

$$z_{LB} = \min \quad \left\{ \sum_{s \in S} p_r(s)(\boldsymbol{c}^\top \boldsymbol{x}^s + \boldsymbol{q}^\top \boldsymbol{y}^{R,s}) : \boldsymbol{x}^1 = \cdots = \boldsymbol{x}^{|S|}, \right.$$
$$\left. (\boldsymbol{x}^s, \boldsymbol{y}^{R,s}) \in \mathrm{conv} \boldsymbol{K}^s, \forall s \in S \right\} \tag{50}$$

Then $z \geqslant z_{LD}^* = z_{LB}^*$.

At the same time, the upper bound on z provided by Eq. (45) is not bigger than the value of solving LP-relaxation of Eq. (43) [23], written as

$$z_{UB} = \min \quad \left\{ \sum_{s \in S} p_r(s)(\boldsymbol{c}^\top \boldsymbol{x}^s + \boldsymbol{q}^\top \boldsymbol{y}^{R,s}) : \boldsymbol{x}^1 = \cdots = \boldsymbol{x}^{|S|}, \right.$$
$$\left. (\boldsymbol{x}^s, \boldsymbol{y}^{R,s}) \in \boldsymbol{K}_{LP}^s, \forall s \in S \right\} \tag{51}$$

where $\boldsymbol{K}_{LP}^s$ arises from $\boldsymbol{K}^s$ without the integer requirements.

As a result,

$$z_{UB} \geqslant z \geqslant z_{LD} := \max_{\boldsymbol{\mu}} \left\{ \sum_{s \in \mathcal{S}} L_s(\boldsymbol{\mu}^s) : \sum_{s \in \mathcal{S}} \boldsymbol{\mu}^s = 0 \right\}.$$

A duality gap may occur between the optimal Lagrangian dual and the optimal value due to the integer requirements. The steps of the modified DD algorithm are shown as Algorithm 1.

IV. NUMERICAL RESULTS

The numerical experiments are performed on IEEE 123-bus distribution system [25]. The capital costs of the proposed ROD methods are shown in Table II, whose life time are assumed to be 30 years. Without considering the interest rate, the annual capital cost for purchasing and installing of each ROD option is $1/30$ of the initial investment cost. It is assumed that the backup DGs are connected in three phase and cannot be installed at the nodes just connected to single or two-phase lines. The basic load shedding cost is assumed to be $\$14/kWh$ [26] and the load shedding cost parameter c_i^L in equation (6) is the product of the basic load shedding cost and the load priority. The repair cost of a single pole for 6 pole types is assumed to be the same ($\chi_{ij,1}^p = \ldots = \chi_{ij,6}^p = \$4000$). The operation cost of backup DGs is assumed to be $\$8kW/h$. The time step is $\Delta t = 2$ hour. It is assumed that there are 5 load priorities, and the voltage range is set to be $0.95 p.u. \sim 1.05 p.u.$ 20 scenarios are randomly generated for experiments. Each

Algorithm 1 The customized DD algorithm

1: ***Initialization:*** Set $z^* = \infty$ and let $\mathcal{G}$ consists of problem (41).

2: ***Termination:*** If $\mathcal{G} = \emptyset$, **then** output $x^\star$ with $z^\star = c^\top x^\star + \mathcal{Q}(x^\star)$ is optimal.

3: ***Node Selection:***
   a) Select and delete a problem $\mathcal{G}_i$ from $\mathcal{G}$
   b) Solve its corresponding Lagrangian dual (48) and its optimal value yields $z_{LD} = z_{LD}(\mathcal{G}_i)$
   c) **If** the associated $z_{LD}(\mathcal{G}_i) = \infty$ (infeasibility of subproblem i) **then** Go to 2.

4: ***Bounding:*** If $z_{LD}(\mathcal{G}_i) \geqslant z^\star_{LD}$, Go to 2. Otherwise proceed as follows:
   If the first-stage solutions $x^s, s \in \mathcal{S}$ of subproblems are
   a) The scenario solutions $x^s, \forall s \in S$ are identical, then set $z^* := \min\{z^*, c^\top x^s + \mathcal{Q}(x^s)\}$ and delete all problems $\mathcal{G}'_i$ with $z_{LD}(\mathcal{G}'_i) \geqslant z^\star_{LD}$ from $\mathcal{G}$. Go to 2.
   b) The scenario solutions $x^s, \forall s \in S$ are different, then compute a suggestion $\hat{x} := Heu(x^1, \ldots, x^{|S|})$ using heuristic (Try solutions of all scenarios). This heuristic is applied in the first 11 nodes to facilitate dicovery of an incumbent early in the B&B tree. **If** $\hat{x}$ is feasible, **then** let $z^* := \min\{z^*, c^\top \hat{x} + \mathcal{Q}(\hat{x})\}$ and delete all problems $\mathcal{G}'_i$ with $z_{LD}(\mathcal{G}'_i) \geqslant z^\star_{LD}$ from $\mathcal{G}$, Go to 5.

5: ***Branching:*** Select a component $x_{(j)}$ of x and add two new problems to $\mathcal{G}$ that differ from $\mathcal{G}_i$ by the additional constraints $x_{(j)} \leqslant \lfloor \hat{x}_{(j)} \rfloor$ and $x_{(j)} \geqslant \lfloor \hat{x}_{(j)} \rfloor + 1$, respectively (as $x_{(j)}$ is integer). Go to 3.

---

scenario is assigned with a probability $p_r(s) = 1/20$. All experiments are implemented on the Iowa State University Condo cluster, whose individual blade consists of two 2.6 GHz 8-Core Intel E5-2640 v3 processors and 128GB of RAM. All models and algorithms are implemented using the software DDSIP [27].

TABLE II
THE INVESTMENT COST OF DIFFERENT ROD METHODS

#No.	Methods	Cost($)
1	Upgrading pole class	6,000/pole
2	Adding transverse guys to pole	4,000/pole
3	The combination of upgrading and guying pole	10,000/pole
3	Installing a natural gas-fired CHPs as DG with 400kW capacity	1,000/kW
4	Adding an automatic sectionlizer	15,000

*Assume the span of two consecutive poles is 150 ft.

A. Comparison with and without ROD

The IEEE 123-bus system is mapped into a coastal city in Texas. According to the histogram of landfall hurricane frequency in Texas [18], it is assumed $w_H = 2$. Fig. 4(a) represents the wind speed experienced by poles, which varies with the pole's distance to the hurricane's eye. Fig. 4(b) compares the pole resistance ($R^3_{ij,n}$) and the wind load $S^3_{ij,n}(t)$. Wind load is determined by the sustained wind speed on the pole. Once $R^3_{ij,n} < S^3_{ij,n}(t_d)$, the pole would be damaged at time t_d and remain damaged until it is repaired, as shown in Fig. 4(c).
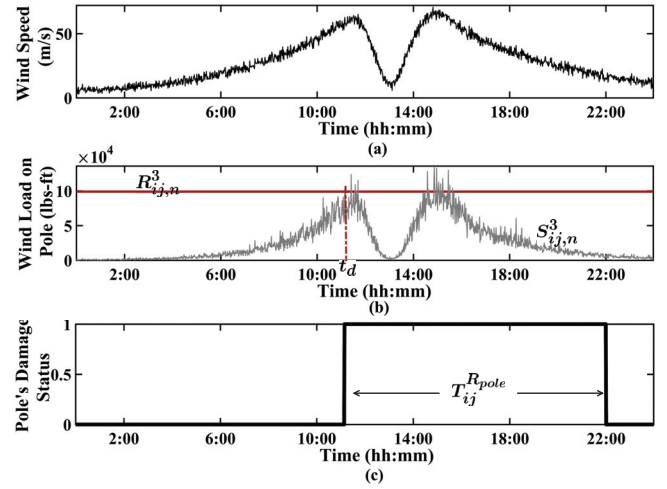

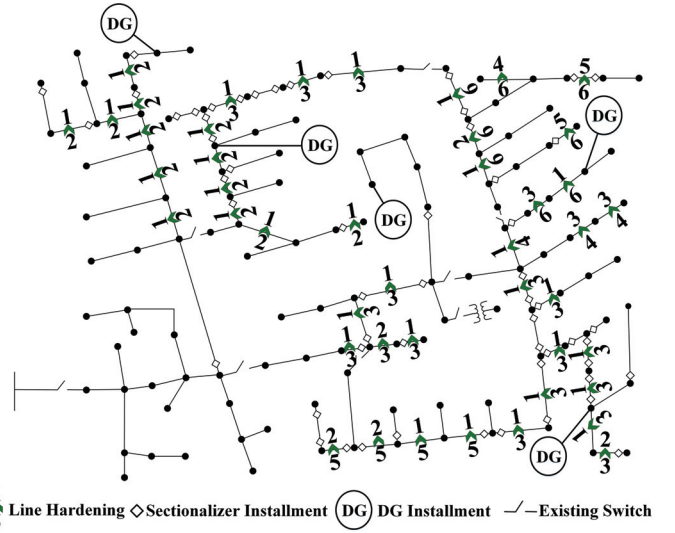Fig. 4. Simulating a distribution pole's damage status in a hurricane

Fig. 5. The optimal ROD methods implementation

When the pole is damaged at time t_d, the entire line is out of service.

We compare the cases with and without ROD under 20 different scenarios to quantify the impact of ROD methods on system resilience. By solving our proposed model, the optimal ROD decisions are shown in Fig 5(b), with a total investment cost of \$5,048,000. Consider the budget limitation, the total number of backup DGs is limited to be 5. We compare the second stage cost from the hurricane hits the system to the point when all damaged lines are repaired as shown in Fig. 6. The expected second-stage cost with optimal ROD is 8.93% of that without ROD. It can seen that the optimal ROD can directly reduce the economic losses during hurricanes.

To further illustrate the effectiveness of ROD, the percentage of power-served (POPS(t)) which can depict the resilience curve against time t is expressed as:

$$\text{POPS}(t) = \sum_{s \in \mathcal{S}} p_r(s) \frac{\sum_{i \in \Omega_N} (1 - y^{r,s}_{i,t}) P^{L,s}_{i,t}}{\sum_{i \in \Omega_N} P^{L,s}_{i,t}}, \forall t \in \mathcal{T}_H \quad (52)$$

Fig. 7 compares system resilience curves with and without
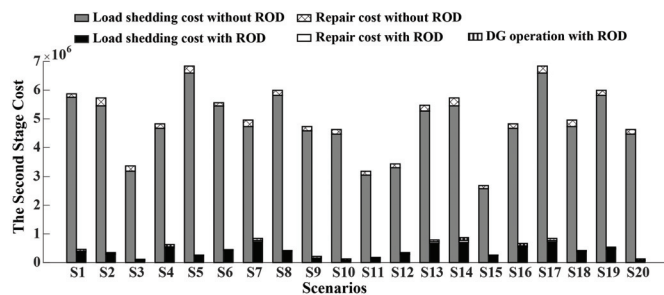
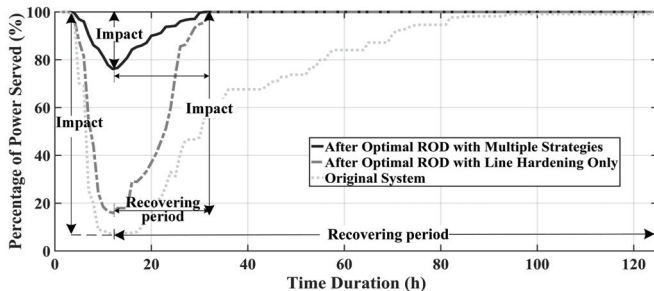Fig. 6. The second stage cost comparison with and without ROD under different scenarios

Fig. 7. The system resilience curve comparison

ROD. Compared to 93% POPS drop in the original system, the system with only optimal line hardening experiences a 84.1% POPS drop and the system after optimal ROD with multiple coordinated ROD options only experiences a 23.9% POPS drop. In addition, the POPS drop starts earlier in the original system. Moreover, systems with optimal ROD have shorter restoration time. For example, the original system needs 112 hours to recover from hurricane, but the systems after optimal ROD only need 20 hours. These results indicate the system with optimal ROD has stronger surviving ability to withstand hurricane and faster recovery. The results also indicate that the DGs and automatic sectionalizers can contribute to mitigating the hurricane's impact on the system. Hence, an optimal ROD should coordinate multiple resilience-enhancing methods.

B. The self-healing operation case

In order to validate the novelty of our MILP formulation strategy to solve the challenges of self-healing operation mentioned in section III-B, the time varying system reactions to a hurricane are analyzed. It is assumed that the distribution system has implemented the optimal ROD measures as Fig. 5(b) shown. We take two operation points at $t = 10$ and $t = 21$ in a scenario as illustrative example. In Fig. 8, there were 14 lines out of service and isolated by the sectionalizers. The distribution system itself sectionalized into 5 healthy islands, which operated as MGs. In each healthy island, there was an active node with zero angle and its network kept radial. The number of zero angles was equal to the number of healthy islands. At the operation point $t = 21$, 6 damaged lines have been repaired. The distribution system reconfigured itself into 3 healthy islands, made some nodes in the de-energized islands become healthy and isolated them from the remaining outage areas as shown in Fig. 9. These results indicate that the proposed modeling strategy can achieve self-healing operation.
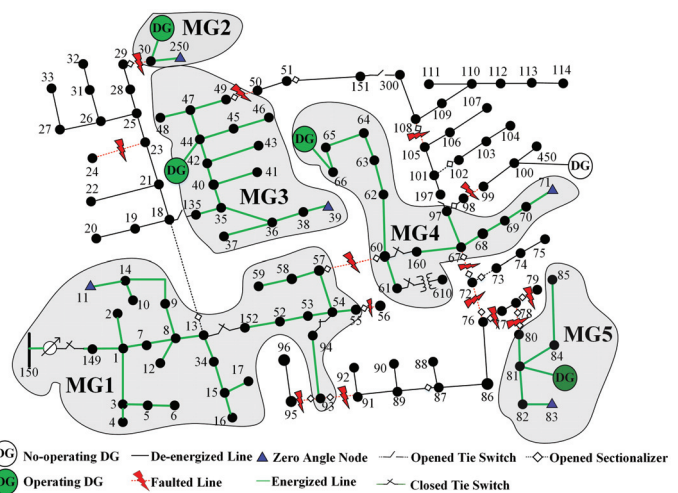

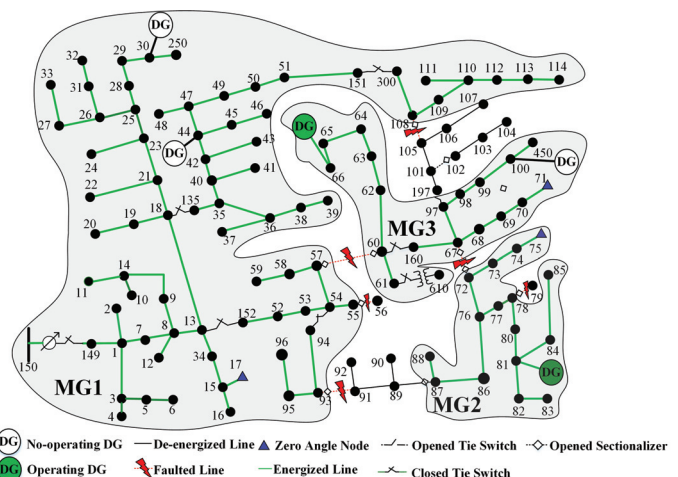Fig. 8. System's self-healing operation at $t = 10$

Fig. 9. System's self-healing operation at $t = 21$

C. Computational Results

Although the DD algorithm can use the branch and bound to converge eventually to any desired gap, it may takes days or weeks for the large scale scale ROD problem to get relative gap at 1% [22]. Here it is assumed the relative optimality gap is 8%. The computational results of ROD problem on the 123-bus test system under different scenarios are shown in the Table III. From Table III, it can been seen that the case with 20 scenarios takes longer computational time to solve but it still can converge to the relative optimality gap 8%.

D. Solution validation

A multiple replication procedure (MRP) [28] is used to test the stability and quality of the candidate solutions shown in Fig. 5. We generate 30 sets of scenarios, and each set has 20 scenarios. The ROD problem is solved for the 30 sets of scenarios to construct the confidence interval (CI) for the optimality gap. The one-sided CI of the candidate solutions as shown in Fig. 5 in the percentage term with regard to the objective value for the optimality gap is $[0, 10.54\%]$. This small gap shows the candidate solutions are stable and of high quality.

TABLE III
THE SOLUTION QUALITY STATICS FOR DD ALGORITHM SOLVING ROD
PROBLEMS

#Scenario	Upper Bound	Lower Bound	Wall Time (h)
5	674,286.3	628,434.8	67
10	729,310.1	671,694.6	115
20	1,057,962.1	976,499.1	156

V. CONCLUSIONS

This paper presents a new modeling and solution methodology for resilience-oriented design (ROD) of power distribution systems against wind-induced climatic hazards. The spatial-temporal correlations among ROD decisions, uncertainty space, and system operations during and after climatic hazards are well explored and established. A two-stage stochastic mixed-integer model is proposed with the objective to minimize the investment cost in the first-stage and the expected costs of the loss of loads, repairs and DG operations in the second stage. To solve this model, a scenario-based dual composition algorithm is developed. Numerical studies on the 123-bus distribution system demonstrate the effectiveness of optimal ROD on enhancing the system resilience: 1) this model can build a resilience curve to represent the ROD decisions' effect on the evolving operation states; 2) the optimal solution of the second stage can model the outage propagation during faults while minimizing the outage areas and preserve radiality in each energized microgrid after reconfiguration. One limitation of the paper is that some detailed features of a real distribution system are not included in the modeling, such as mixed-phase unbalanced operation and mixed transformer connections. In future work, we will consider multiple extreme events and detailed features of practical distribution systems, and design more computationally efficient solution algorithms.

REFERENCES

[1] A. Gholami, F. Aminifar, and M. Shahidehpour, "Front lines against the darkness: enhancing the resilience of the electricity grid through microgrid facilities," *IEEE Electrif. Mag.*, vol. 4, no. 1, pp. 18–24, 2016.

[2] "Economic benefits of increasing electric grid resilience to weather outages," White House, Tech. Rep., Jul. 2013.

[3] M. Panteli and P. Mancarella, "The grid: Stronger, bigger, smarter?: Presenting a conceptual framework of power system resilience," *IEEE Power Energy Mag.*, vol. 13, no. 3, pp. 58–66, May 2015.

[4] M. Panteli, D. N. Trakas, P. Mancarella, and N. D. Hatziargyriou, "Power systems resilience assessment: Hardening and smart operational enhancement strategies," *Proceedings of the IEEE*, vol. 105, no. 7, pp. 1202–1213, Jul. 2017.

[5] A. Gholami, T. Shekari, M. H. Amirioun, F. Aminifar, M. H. Amini, and A. Sargolzaei, "Toward a consensus on the definition and taxonomy of power system resilience," *IEEE Access*, vol. 6, pp. 32 035–32 053, 2018.

[6] A. Arab, A. Khodaei, S. K. Khator, K. Ding, V. A. Emesih, and Z. Han, "Stochastic pre-hurricane restoration planning for electric power systems infrastructure," *IEEE Trans. Smart Grid*, vol. 6, no. 2, pp. 1046–1054, Mar. 2015.

[7] M. H. Amirioun, F. Aminifar, and H. Lesani, "Resilience-oriented proactive management of microgrids against windstorms," *IEEE Trans. Power Syst.*, vol. PP, no. 99, p. 1, 2017.

[8] H. Gao, Y. Chen, S. Mei, S. Huang, and Y. Xu, "Resilience-oriented pre-hurricane resource allocation in distribution systems considering electric buses," *Proc. IEEE*, vol. 105, no. 7, pp. 1214–1233, Jul. 2017.

[9] C. Chen, J. Wang, F. Qiu, and D. Zhao, "Resilient distribution system by microgrids formation after natural disasters," *IEEE Trans. Smart Grid*, vol. 7, no. 2, pp. 958–966, Mar. 2016.

[10] A. Arif, Z. Wang, J. Wang, and C. Chen, "Power distribution system outage management with co-optimization of repairs, reconfiguration, and DG dispatch," *IEEE Trans. Smart Grid*, vol. PP, no. 99, p. 1, 2017.

[11] W. Yuan, J. Wang, F. Qiu, C. Chen, C. Kang, and B. Zeng, "Robust optimization-based resilient distribution network planning against natural disasters," *IEEE Trans. Smart Grid*, vol. PP, no. 99, pp. 1–10, 2016.

[12] S. Ma, B. Chen, and Z. Wang, "Resilience enhancement strategy for distribution systems under extreme weather events," *IEEE Trans. Smart Grid*, vol. PP, no. 99, p. 1, 2016.

[13] E. Yamangil, R. Bent, and S. Backhaus, "Resilient upgrade of electrical distribution grids," in *Twenty-Ninth AAAI Conference on Artificial Intelligence*, Austin, Texas, USA, Jan. 2015, pp. 1233–1240.

[14] S. Ma, L. Su, Z. Wang, F. Qiu, and G. Guo, "Resilience enhancement of distribution grids against extreme weather events," *IEEE Trans. Power Syst.*, 2018.

[15] R. W. Wolfe and R. O. Kluge, "Designated fiber stress for wood poles," *Gen. Tech. Rep. FPL-GTR-158. Madison, WI: US Department of Agriculture, Forest Service, Forest Products Laboratory. 39 p.*, vol. 158, 2005.

[16] S. Bjarnadottir, Y. Li, and M. G. Stewart, "Hurricane risk assessment of power distribution poles considering impacts of a changing climate," *J. Infrastruct. Syst.*, vol. 19, no. 1, pp. 12–24, 2012.

[17] N. G. B. III, "ANSI-NESC update," 2005 AWPA Annual Meeting, Tech. Rep., 2005. [Online]. Available: http://woodpoles.org/portals/2/documents/ANSI_NESC_05.pdf

[18] R. Brown, "Cost-benefit analysis of the deployment of utility infrastructure upgrades and storm hardening programs," *Quanta Technology, Raleigh, NC*, 2009.

[19] S. Ma, S. Li, Z. Wang, A. Arif, and K. Ma, "A novel MILP formulation for fault isolation and network reconfiguration in active distribution systems," in *Proc. IEEE Power Energy Society General Meeting (PESGM)*, Portland, Oregon, USA, Aug. 2018, pp. 1–5.

[20] R. K. Ahuja, T. L. Magnanti, and J. B. Orlin, "Network flows: theory, algorithms, and applications," 1993.

[21] M. E. Baran and F. F. Wu, "Network reconfiguration in distribution systems for loss reduction and load balancing," *IEEE Trans. Power Delivery*, vol. 4, no. 2, pp. 1401–1407, Apr. 1989.

[22] D. Gade, G. Hackebeil, S. M. Ryan, J.-P. Watson, R. J.-B. Wets, and D. L. Woodruff, "Obtaining lower bounds from the progressive hedging algorithm for stochastic mixed-integer programs," *Math. Program.*, vol. 157, no. 1, pp. 47–67, 2016.

[23] G. Guo, G. Hackebeil, S. M. Ryan, J.-P. Watson, and D. L. Woodruff, "Integration of progressive hedging and dual decomposition in stochastic integer programs," *Oper. Res. Lett.*, vol. 43, no. 3, pp. 311–316, 2015.

[24] G. L. Nemhauser and L. A. Wolsey, "Integer programming and combinatorial optimization," *Wiley, Chichester. GL Nemhauser, MWP Savelsbergh, GS Sigismondi (1992). Constraint Classification for Mixed Integer Programming Formulations. COAL Bulletin*, vol. 20, pp. 8–12, 1988.

[25] W. H. Kersting, "Radial distribution test feeders," in *Power Engineering Society Winter Meeting*, vol. 2. IEEE, pp. 908–912.

[26] R. E. Brown, *Electric power distribution reliability*. Boca Raton: CRC press, 2008.

[27] A. Märkert and R. Gollmer, "Users guide to ddsip–ac package for the dual decomposition of two-stage stochastic programs with mixed-integer recourse," *Department of Mathematics, University of Duisburg-Essen, Duisburg*, 2008.

[28] G. Bayraksan and D. P. Morton, "Assessing solution quality in stochastic programs via sampling," *Tutorials in Operations Research*, vol. 5, pp. 102–122, 2009.

Shanshan Ma (S'14) is currently working toward a Ph.D. degree with the Department of Electrical & Computer Engineering at Iowa State University, Ames, IA, USA.

Shiyang Li (S'08-M'16) is a researcher with the State Key Laboratory of HVDC, Electric Power Research Institute, CSG, Guangzhou, China. He received the Ph.D. degrees in electrical and computer engineering from Iowa State University in 2017.

Zhaoyu Wang (S'13-M'15) is the Harpole-Pentair Assistant Professor with Iowa State University, Ames, IA, USA. He received the M.S. and Ph.D. degrees in electrical and computer engineering from Georgia Institute of Technology in 2012 and 2015, respectively.

Feng Qiu (M'14) received his Ph.D. from the School of Industrial and Systems Engineering at the Georgia Institute of Technology in 2013. He is a computational scientist with the Energy Systems Division at Argonne National Laboratory, Argonne, IL, USA.